Eccentricity-tide coupling: Impact on binary neutron stars and extreme mass ratio inspirals

John Paul Bernaldez[*] and Sayak Datta[†]

*Max-Planck-Institut für Gravitationsphysik (Albert-Einstein-Institut), D-30167 Hannover, Germany
and Leibniz Universität Hannover, D-30167 Hannover, Germany*

We study the effect of tidal interaction between two compact bodies in an eccentric orbit. We assume the tidal fields to be static. Therefore, we ignore the dynamic tides and resonant excitations. Using the results, we find the analytical expression for the phase shift of the emitted gravitational wave. In the process, we find that in the leading order, the initial eccentricity e_0 and the dimensionless tidal deformability Λ couple as $\sim e_0^n \Lambda$, where n is a positive number. We only focus on the dominant contribution, i.e., $e_0^2 \Lambda$. We also compute the accumulated dephasing for binary neutron star systems. We find that for optimistic values of eccentricities $e_0 \sim 0.05$ and $\Lambda \sim 600$, the accumulated dephasing is $\mathcal{O}(10^{-4})$ radian, requiring a signal-to-noise ratio ~ 7000 to be observable. Therefore, these effects can be measured in binary neutron star systems with large eccentricities if the signal-to-noise ratios of the systems are also very large. Hence, in third-generation detectors, it may have an observable impact if the systems have large eccentricities. We also explore the impact of this effect on extreme mass-ratio inspirals (EMRIs). We find that even for supermassive bodies with small values of $\Lambda \sim 10^{-3}$, this effect has large dephasing in EMRIs $\sim \mathcal{O}(10)$ radian. Therefore, this effect will help in probing the nature of the supermassive bodies in an EMRI.

I. INTRODUCTION

The recent detection of gravitational waves (GWs) by LIGO [1]/Virgo [2] (LVC) collaboration from two binary neutron star (BNS) merger event named GW170817 [3,4] and GW190425 [5] has ushered in a new light for constraining the equation of state (EOS) of neutron stars (NSs) [4,6,7]. The tidally deformed components of a BNS merger in their late inspiral phase leave a detectable imprint on the emitted GW signals. These imprints depend on the EOS of neutron stars [8–11]. The measurement of the tidal deformability associated with these observations, therefore, provides direct information about the equation of state of the NS [8–11]. Thus, one can use this imprint to study the properties of dense matter far from the nuclear saturation density. The tidal deformability of an NS does not only depend on the EOS of the matter inside the star but also on the fluid nature of the matter [12–16]. Therefore, the information contained in the tidal deformability is very rich. Apart from GWs, other types of astrophysical observations also have supplied complementary constraints on the properties of NSs. Space-based mission led by Neutron Star Interior Composition ExploreR (NICER) collaboration has already presented a quite precise measurement of mass and radius of PSR J0030 + 0451 [17,18] and PSR J0740 + 6620 [19,20] using pulse-profile modeling. Additionally, observations of massive pulsars [21–23] by radio telescopes provide important insights on the high-density part of the NS EOS. All of these measurements of NS macroscopic properties, such as mass (M), radius (R), and tidal deformability (λ), lead us to the EOS which is the same for all the NSs present in the universe.

To measure these macroscopic properties, the waveform models have been constructed under the approximation of circular orbits. Theoretically, it is expected that BNSs get circularized by the time it enters the observable band. Even if it retains some eccentricity, it is expected to be small. The measurement of the eccentricities in the observed systems is consistent with such expectations [24,25]. For these reasons tidal interactions in BNSs got attention primarily for the circular orbit. In Ref. [8], for the first time, the impact of the tidal deformability on the emitted GW from a circular orbit binary was calculated. Then, these results were extended, taking considerations of higher post-Newtonian corrections [26–30]. The initial works primarily focused on the impact of the static tides. However, these were also extended to address the dynamic tides and

[*]john.bernaldez@aei.mpg.de
[†]sayak.datta@aei.mpg.de

resonant excitations [8,31–34]. In Refs. [35–38], the impact of the spin of NSs has been explored. The proposed 3rd generation (3G) GW detectors, Einstein Telescope (ET) and Cosmic Explorer (CE) will have a higher sensitivity than current detectors, which will result in higher signal-to-noise ratio (SNR) for BNSs [39,40]. In light of that, these effects are being explored for observational purposes. In Refs. [41–44], the tidal interactions in the presence of eccentricities have also been explored in a very general setting. These works primarily focused on numerically studying the properties of this interaction and computing resonant excitations.

In this paper, we focus on studying the impact of tidal deformability in eccentric orbits. However, we invest in a much simpler project. We would like to compute the impact of eccentricity in the presence of a static tide. Under such assumptions, we will derive analytical expressions for orbital energy, GW flux, and also the modified expression for phase. As a result, this expression can be used for parameter estimation purposes. Since it is expected that the orbits will get circularized when it enters the observable band, we expect that the eccentricity will contribute primarily in the earlier part of the inspiral. Therefore, the assumption of the static tide is very close to reality, as far as the BNSs are concerned. However, once the expressions are found, we will also explore the impact on other sources for exploration purposes. We work in the unit $G = c = 1$.

II. TIDAL LOVE NUMBER

Consider a static, spherically symmetric star of mass m placed in an external quadrupolar tidal field $\mathcal{E}_{ij}$. In response to the external tidal field, the star will develop an induced quadrupole moment Q_{ij}. The induced quadrupole moment depends on both the external tidal field and the properties of matter inside the star. This, as a result, affects the metric of the star. In the star's local asymptotic rest frame (asymptotically mass centered Cartesian coordinates) at large r, the metric coefficient g_{tt} is given by (in units with $G = c = 1$):

$$\frac{1 - g_{tt}}{2} = -\frac{m}{r} - \frac{3Q_{ij}}{2r^3}\left(n^i n^j - \frac{1}{3}\delta_{ij}\right) + \frac{1}{2}\mathcal{E}_{ij}x^i x^j, \quad (1)$$

where $n^i = x^i/r$. This expansion is used to define the traceless tensors Q_{ij} and the tidal field $\mathcal{E}_{ij}$. To linear order in static case, the induced quadrupole will be of the form

$$Q_{ij} = -\lambda \mathcal{E}_{ij}. \quad (2)$$

Here, λ is a constant, namely tidal deformability. It is connected to the dimensionless tidal Love number $k_2 = \frac{3}{2}\lambda R^{-5}$, where R is the radius of the star. In the linear approximation, the relation between $\mathcal{E}_{ij}$ and Q_{ij} defines the

tidal deformability λ. Hence, the details of the quadrupolar structure mimic the external tidal field, via $\mathcal{E}_{ij}$, and λ captures the response of the body. This approximation, however, is valid only when the tide is considered to be static, i.e., orbital timescale is much larger than the time-scale of the star's internal dynamics. This approximation breaks down in the late inspiral and necessitates including the dynamic nature of the tidal field. This is called the dynamic tide, which we will leave for future study. As the star's internal response is captured through λ, it heavily depends on the EOS of the star. The measurement of λ from GW astronomy has already provided us with information regarding the EOS of the NSs. In the future, with more sensitive detectors, it is expected to provide us with further details in a precise manner. Therefore, it is of utmost importance to accurately model the contribution. In the next sections, we will explore these effects in a general setting.

III. EQUATION OF MOTION IN THE PRESENCE OF A TIDAL FIELD

In this section, we will focus on deriving orbital equations of motions and their solutions. We consider a binary with component masses m_i and tidal deformabilities λ_i, where $i = 1, 2$. Similar to Ref. [8], for simplicity, we compute only the effects on the first body. For the total contribution of both the bodies, a similar contribution can be added for the second body by interchanging the labels $(1 \leftrightarrow 2)$. In the phase of the emitted GW, the signals from the two stars simply get added. The action of such systems can be expressed as,

$$S = \int dt \left[\frac{1}{2}\mu \dot{r}(t)^2 + \frac{1}{2}\mu r(t)^2 \dot{\phi}(t)^2 + \frac{M\mu}{r(t)}\right] - \left\{\frac{1}{2}\int dt Q_{ij}\mathcal{E}_{ij}\right.$$
$$\left. - \sum_n \int dt \frac{1}{4\lambda_{1,n}\omega_n^2}[\dot{Q}_{ij}^{(n)}\dot{Q}_{ij}^{(n)} - \omega_n^2 Q_{ij}^{(n)}Q_{ij}^{(n)}] + 1 \leftrightarrow 2\right\}, \quad (3)$$

where M and μ are the total and reduced mass of the system, and $\mathcal{E}_{ij} = -m_2 \partial_i \partial_j (1/r)$ is the tidal field. $Q_{ij}^{(n)}$ and $\lambda_{1,n}$ are the contribution to the total induced quadrupole moment Q_{ij} and tidal deformability, respectively. Alongside, $\lambda_1 \equiv \sum_n \lambda_{1,n}$ and $Q_{ij} \equiv \sum_n Q_{ij}^{(n)}$. The relative displacement is written as, $\mathbf{x} = (r\cos\phi, r\sin\phi, 0)$.

This form of action was considered in Ref. [8] to find the contributions of the different frequencies of the modes. However, the mode frequencies contribute in the very late inspiral stages. It is well known that the eccentricities of a binary system decreases with increasing frequency. Therefore, the dominant contribution in the eccentric orbit will come from the initial phase of the inspiral. The frequency ω in that phase is much smaller than the mode frequencies ω_n of the stars, i.e. $\omega_n \gg \omega$. For this purpose, we will ignore such contributions.

Unlike in Ref. [8] we will vary the action with respect to r, ϕ, and $Q_{ij}^{(n)}$. The resulting equations are as follows,

$$\mu\ddot{r}(t) = \mu r(t)\dot{\phi}(t)^2 - \frac{M\mu}{r(t)^2} - \frac{1}{2}Q_{ij}\frac{\partial\mathcal{E}_{ij}}{\partial r} \qquad (4)$$

$$\frac{d}{dt}(\mu r^2\dot{\phi}) = -\frac{1}{2}Q_{ij}\frac{\partial\mathcal{E}_{ij}}{\partial\phi} \qquad (5)$$

$$\ddot{Q}_{ij}^{(n)} + \omega_n^2 Q_{ij}^{(n)} = m_2\lambda_{1,n}\omega_n^2\partial_i\partial_j\frac{1}{r}. \qquad (6)$$

In the current scenario, we consider that the mode frequency does not contribute. This eventually implies that the time variation of quadrupole moment is very small, i.e. $\ddot{Q}_{ij}^{(n)} \ll \omega_n^2 Q_{ij}^{(n)}$. Therefore, Eq. (6) simplifies to,

$$Q_{ij}^{(n)} = m_2\lambda_{1,n}\partial_i\partial_j\frac{1}{r} \qquad (7)$$

and, as a result, it boils down to Eq. (2), $Q_{ij} = -\lambda\mathcal{E}_{ij}$. We will use this result throughout the paper. With the solution of $Q_{ij}^{(n)}$ Eq. (4) can be simplified as follows:

$$\mu\ddot{r}(t) = \mu r(t)\dot{\phi}(t)^2 - \frac{M\mu}{r(t)^2} - \frac{9m_2^2\lambda_1}{r(t)^7}. \qquad (8)$$

In Eq. (5), it is noteworthy that angular momentum is not conserved unless the right-hand side vanishes. However, in case of static tide due to Eq. (2), the right-hand side of the equation vanishes and the angular momentum is conserved. This may not be true in general and in the range $\omega \sim \omega_n$. This aspect needs to be explored in the future (Check Ref. [43] for a general approach).

It is easier to solve Eq. (8) by reexpressing the time variation of radius in terms of the time variation with ϕ. Hence, we use,

$$\dot{r} = \frac{dr}{d\phi}\dot{\phi}. \qquad (9)$$

Using the above equation, Eq. (8) takes the following form,

$$\frac{d^2r}{d\phi^2}\mu^2r^4\dot{\phi}^2 - 2\mu^2r^3\dot{\phi}^2\left(\frac{dr}{d\phi}\right)^2 = \mu^2r^5\dot{\phi}^2 - M\mu^2r^2 - \frac{9\mu m_2^2\lambda_1}{r^3} \qquad (10)$$

Except the last term in the right-hand side, the equation is similar to the equation of a gravitating body. The last term represents the leading order tidal interaction.

In the absence of a tidal field we can take the limit $(\lambda_1 \to 0)$, and the solution satisfies an equation of ellipse,

$$r = \frac{a(1 - e^2)}{(1 + e\cos\phi)}, \qquad (11)$$

where a and e are the semimajor axis and eccentricity, respectively. We will assume that the effect of the tidal field is perturbative in nature. Therefore, the corresponding solution can be treated as a perturbation compared to the leading contribution. With this, we can replace $\dot{\phi}$ using the leading order expression of eccentric orbit, $\dot{\phi} = \omega(1 - e^2)^{-3/2}(1 + e\cos(\phi))^2$ [45,46].

Thus, we obtain:

$$-(1 - e^2)^3(9m_2^2\lambda_1 + M\mu r^5) + (1 + e\cos\phi)^4$$
$$\times\left(\mu\omega^2r^8 + 2\mu\omega^2r^6\left(\frac{dr}{d\phi}\right)^2 - \mu\omega^2r^7\frac{d^2r}{d\phi^2}\right) = 0, \qquad (12)$$

We will use this equation to find the solution of the orbital motion. The solution of this equation will contain both the leading order solution $(\lambda_1 = 0)$ and the perturbative correction due to the tide. To separate out the perturbation, we use the ansatz:

$$r(\omega, \phi, e) = \frac{M^{1/3}\omega^{-2/3}(1 - e^2)}{(1 + e\cos\phi)}(1 + \gamma\bar{\delta r}(\phi, e)), \qquad (13)$$

where $\bar{\delta r}$ corresponds to perturbation in radius and $\gamma = \frac{3m_2^2\lambda_1\omega^{10/3}}{\mu M^{8/3}}$, and $\omega = a^{-3/2}M^{1/2}$ is the average orbital frequency. Note, that in the absence of the tidal field the above equation boils down to an eccentric orbit. Also, note that we have scaled out a factor proportional to the leading order solution from the perturbation for clarity as well as brevity. The coefficient γ depends both on the tidal deformability as well as on ω. Therefore the perturbative part is by construction in higher post-Newtonian order. Using the ansatz, we find the equation for $\bar{\delta r}$ to be

$$(1 - e^2)^5(1 + e\cos\phi)\frac{d^2\bar{\delta r}}{d\phi^2} - 2e(1 - e^2)^5\sin\phi\frac{d\bar{\delta r}}{d\phi}$$
$$- 3(1 - e^2)^5\bar{\delta r} + 3(1 + e\cos\phi)^5 = 0 \qquad (14)$$

Note, that the above equation is now free of ω. We expand this equation in series of e and keep up to the e^2 term. Then, it is straight forward to find the solution to be,

$$\bar{\delta r} = 1 + e\frac{15}{4}\cos\phi + e^2\left(\frac{85}{8} + \frac{75}{56}\cos(2\phi)\right). \qquad (15)$$

The final expression of r with e is given by

$$r(\omega, \phi, e) = \frac{M^{1/3}\omega^{-2/3}(1-e^2)}{(1+e\cos\phi)}\left\{1+\gamma\left[1+e\frac{15}{4}\cos\phi\right.\right.$$
$$\left.\left. + e^2\left(\frac{85}{8}+\frac{75}{56}\cos 2\phi\right)\right]\right\}. \quad (16)$$

This result will be used in the paper to find the GW contributions. Note, in the circular limit ($e = 0$), the result exactly reproduces the result derived in Ref. [8].

IV. IMPACT ON THE EMITTED GW

In the last section, we derived the solution of orbital motion in the presence of a tidal field. In this section, we want to compute the impact of this on the emitted GW from the system. The impact on the GW is computed by considering the change in the inspiral rate, which depends on the emitted GW flux from an orbit. With the loss of energy, the orbits shrink to reach a merger. Due to the tidal interaction, as the orbital structures get modified, so do their energy content and quadrupolar structure. The total energy of the system at an instant can be determined by computing the Hamiltonian (H) of the system. Once, the Hamiltonian is known we compute an orbital average to find the average energy $E = \langle H \rangle$.

To compute average over any quantity, say $X(\phi)$, we average over orbital time period (T). Then using the relation between time and ϕ this averaging can be translated over to an average over ϕ as follows [45,46]:

$$\langle X \rangle \equiv \int_0^T \frac{dt}{T} X = (1-e^2)^{3/2}\int_0^{2\pi}\frac{d\phi}{2\pi}(1+e\cos\phi)^{-2}X(\phi). \quad (17)$$

This, as a result, will give us the expression of the energy of the system at an inspiral instant [8].

$$E = -\frac{1}{2}\mu M^{2/3}\omega^{2/3}\left(1 - \gamma\left(3 + \frac{55}{2}e^2\right)\right). \quad (18)$$

For $e = 0$, Eq. (18) matches with Ref. [8] in static tide limit.

The energy emitted through GW can be computed from the time variation of the total quadrupole moment of the system,

$$Q_{ij}^T = Q_{ij} + \mu x_i x_j. \quad (19)$$

The total power radiated from the system can be obtained using the time derivatives of quadrupole moment in the following manner [45]:

$$\dot{E} = -\frac{1}{5}\left\langle\frac{d^3 Q_{ij}^T}{dt^3}\frac{d^3 Q_{ij}^T}{dt^3} - \frac{1}{3}\frac{d^3 Q_{ii}^T}{dt^3}\frac{d^3 Q_{jj}^T}{dt^3}\right\rangle, \quad (20)$$

where $\langle\rangle$ represents the orbital average, and the repeated indices have been summed over. Substituting the equations for Q_{ij}^T, we obtain:

$$\dot{E} = -\frac{32}{5}\mu^2 M^{4/3}\omega^{10/3}\left[1 + 2\gamma\left(2 + \frac{M}{m_2}\right) + e^2\bar{P}_1\right], \quad (21)$$

where,

$$\bar{P}_1 = \frac{157}{24} + \gamma\left(\frac{371}{3} + \frac{279}{4}\frac{M}{m_2}\right) \quad (22)$$

With the emission of a gravitational wave, the binary loses its energy and inspirals inward. This, as a result, changes the energy of the system in the radiation reaction timescale. Along with modifying the energy, this also changes the eccentricity of the orbit. Therefore, to compute the impact of the inspiral, it is required to know the evolution of eccentricity to the GW frequency. From the knowledge of flux, the eccentricity evolution has been computed in several works. The evolving eccentricity can be expressed in terms of the frequency and initial eccentricity e_0. In the leading order, it follows [46],

$$e(f) = e_0\left(\frac{f_0}{f}\right)^{19/18}, \quad (23)$$

where e_0 is the eccentricity at $f = f_0$. For the point particle configuration where the tidal field vanishes, at an instant of inspiral, a post-Keplerian approach is taken. The eccentricity e and the mean motion n are written in terms of the orbital energy and angular momentum. Using such expressions and along with the fluxes, eccentricity evolution is computed in terms of f [46,47]. Since tidal deformability contributes at post-5-Newtonian order, it will result in an additional corresponding contribution to de/df of the point particle result. Ideally, a post-Keplerian approach should be constructed even in the presence of the tide. It as a consequence will modify Eq. (23). However, in the current work, we will ignore such modification and will consider only the leading order term in the eccentricity evolution. Nevertheless, it is important to find the modification via a post-Keplerian approach and add the corresponding contribution. We leave such details for future work.

At this point, we are equipped to compute the phase contribution due to tidal effects. The expression of energy, flux, and eccentricity can be used to find the phase of the Fourier transform of the GW signal using the following equation:

$$\frac{d^2\Psi}{df^2} = \frac{2\pi}{\dot{E}}\frac{dE}{df} \quad (24)$$

This equation can be integrated using the expression of energy, flux, and eccentricity evolution. As a result, it is possible to express the phasing in a series expansion of GW frequency (f). We find the dephasing due to the tidal effect as follows:

$$\delta\Psi_T = \frac{-3}{128\,\mu M^{2/3} f^{5/3}\pi^{5/3}}\left[\left(\frac{24m_2\pi^{10/3}f^{10/3}(11m_2+M)}{\mu M^{8/3}} + \frac{45m_2\pi^{10/3}f_0^{19/9}e_0^2(378m_2+523M)f^{11/9}}{26\,\mu M^{8/3}}\right)\lambda_1 + 1\leftrightarrow 2\right], \quad (25)$$

where T in $\Psi_T(f)$ represents the tidal part of the phase. The first term is similar to the result found in Ref. [8] corresponding to the circular orbits. The second term represents the correction due to eccentricity. Defining the mass-ratio $q = \frac{m_1}{m_2}$, we can express the phase as:

$$\delta\Psi_{e_0,\lambda} = \frac{-135\pi^{5/3}f_0^{19/9}e_0^2}{3328(1+q)^2\mu^2 M^{4/3}f^{4/9}}$$
$$\times [(901+523q)\lambda_1 + (901q^2+523q)\lambda_2]. \quad (26)$$

This expression will be used in the next sections to compute the impact on the GW.

V. OBSERVATIONAL IMPACT

In the preceding sections, we delved into the orbital dynamics influenced by a tidal field, ultimately deriving expressions for the phase modification of the emitted gravitational waves (GWs) in such systems. Now, we will shift our focus to various types of systems where these contributions could hold significance. Although the dephasing expression was initially derived under the assumption of very small eccentricities, in subsequent sections, we will extrapolate its applicability even to cases with larger eccentricities. It is essential to note that these extrapolations may not strictly align with the model's domain of validity, but they serve as guiding insights into potential scenarios where these phenomena could have observable effects. Therefore, these results should be interpreted as indicative in nature, motivating further in-depth investigations.

A. Binary neutron star

Binary neutron star (BNS) sources are most interesting in the context of tidal deformability. From the observation of GW170817 and GW190425, it has been possible to measure dimensionless tidal deformability ($\Lambda_i m_i^5 \equiv \lambda_i$) and, as a result, put a constraint on $\Lambda_{1.4M_\odot}$ [48,49]. This, as a result, has shed light on the EOS of NS matter. It has also been possible to put an upper bound on the eccentricity of these systems [24,25]. From the theoretical understanding, as well as from the limited observations, we expect BNS systems to have very small eccentricities. It is expected that these systems will get circularized before entering the observable bands. Therefore, we do not expect the contribution of eccentricity-tide coupling in Eq. (26) to contribute significantly. However, in a few recent studies, the possibility of forming eccentric

compact binaries in the LIGO band by resonant and hierarchical triple and quadruple systems in globular clusters has been explored [50–57]. In Ref. [58], dynamically captured binaries have also been explored. Although these events could be rare, they contain information about the formation channels, environment, and distribution. With the advent of third-generation detectors such as the Einstein telescope and cosmic explorer, there is a possibility of measuring small values of dephasing at large signal-to-noise ratio (SNR). Therefore it might be possible to observe BNSs with small nonzero eccentricity, shedding light on the possible formation channels. For this purpose, we will study these systems here.

To study the impact, we plot $\delta\Psi_{e_0,\lambda}$ from Eq. (26). The systems have been considered to be comprised of two equal mass NSs with $m_1 = m_2 = 1.4M_\odot$. The initial eccentricities e_0 of the systems are $e_0 = 0.05$, 0.1, 0.2, and 0.4. Initial eccentricity has been defined at $f_0 = 10$ Hz. The frequency interval for the plots is from $f_i = 4$ Hz up to $f_{\rm ISCO}$, which refers to the frequency at the innermost stable circular orbit (ISCO). We used Ref. [59] for the expression of ISCO frequency in BNS system. The figures have been represented in terms of dimensionless Love number $\lambda_i = \Lambda_i(m_i)^5$. The Λ values taken for the system are $\Lambda = 400$ and 600.

The plots for the eccentricity-tide coupling term of the gravitational wave phase, $\delta\Psi_{e_0,\lambda}$, for $\Lambda = 400$ as a function of gravitational wave frequency f is shown in Fig. 1(a). From the plots, it can be seen that taking larger gravitational wave frequencies correspond to a smaller phasing. This is because the eccentricity of a binary is not a fixed quantity. It decreases with increasing frequency. This results in an overall decreasing pattern of the phase. It can also be seen that larger e_0 corresponds to a larger phase difference, such as for $e_0 = 0.4$ and 0.2. On the other hand, the contribution to the phase difference for small values of e_0, such as for values 0.05 and 0.1, is very small. This is also understandable since $\delta\Psi_{e_0,\lambda} \propto e_0^2$. In addition, not only does the coupling contribution decreases for larger gravitational wave frequencies, but also the value of phase is very small even at earlier frequencies. This implies that the e_0 has smaller contributions to the tidal perturbation as a whole.

In Fig. 1(b), we show the plots for $\Lambda = 600$. From the plots, we can see that similar observations apply, where the large values of initial eccentricities correspond to a larger contribution to the phase difference of the gravitational wave. However, when comparing to $\Lambda = 400$, we can see that for $\Lambda = 600$, the tidal perturbation contribution is
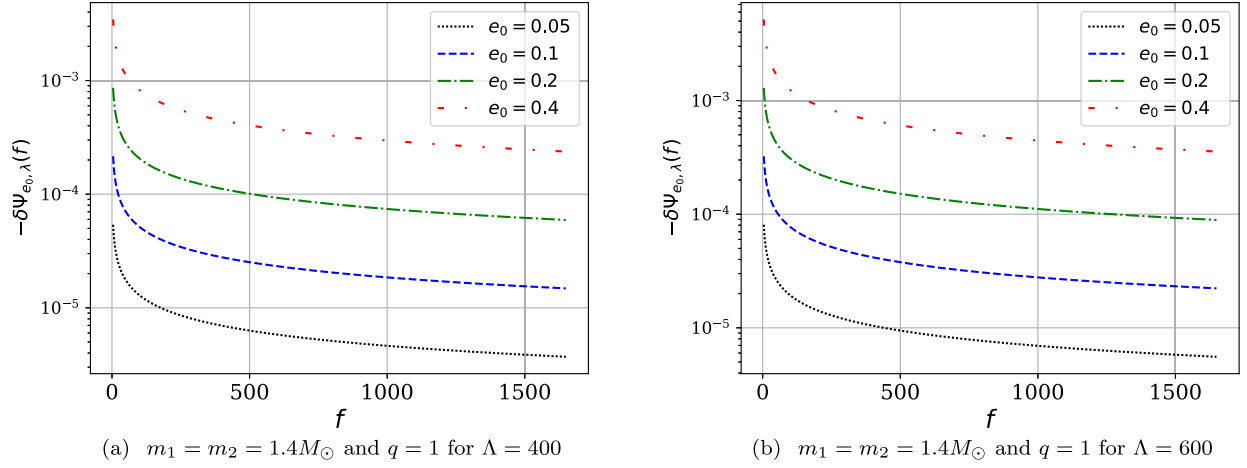
(a) $m_1 = m_2 = 1.4 M_\odot$ and $q = 1$ for $\Lambda = 400$

(b) $m_1 = m_2 = 1.4 M_\odot$ and $q = 1$ for $\Lambda = 600$

FIG. 1. We show the phasing $-\delta\Psi_{e_0,\lambda}$ (in radian) for a binary with two $1.4 M_\odot$ neutron stars as a function of gravitational wave frequency f in the range $f_i = 4$ Hz to f_{ISCO}. The initial eccentricities taken for the figure are $e_0 = 0.05, 0.1, 0.2$, and 0.4 with $\Lambda_1 = \Lambda_2 = \Lambda = 400$ and 600 respectively.

higher for the same values of e_0. This is because $\delta\Psi_{e_0,\lambda} \propto \Lambda$, however, overall the contributions are very small.

In Fig. 2, we plot for $\delta\Psi_T$ to compare the effect of eccentricity with the whole phase due to tidal deformability. We plot for (a) $\Lambda = 400$ and (b) $\Lambda = 600$ and initial eccentricities $e_0 = 0.05, 0.1, 0.2$, and 0.4. The values of e_0 appear to have smaller contributions to the total tidal phase, especially on the larger frequencies. Even larger values of e_0, which initially have a notable contribution, as shown in Fig. 1 turn out to have smaller contributions comparatively. However, we see a notable increase on the slope from $\Lambda = 400$ to $\Lambda = 600$, which is consistent from Fig. 1, where a larger Λ has a larger effect on the phase difference. It implies that e_0 only has significant contributions when taking smaller gravitational wave frequencies. Otherwise the overall structure has similar behavior as found in

Ref. [60], which shows the tidal perturbations as a function of gravitational wave frequency for circular orbits.

In Fig. 3 we demonstrate the accumulated dephasing $-\delta\phi$ as a function of Λ for an equal mass nonspinning binary neutron stars. This represents the total dephasing accumulated in a given frequency band. This is given by:

$$\delta\phi = \int_{f_i}^{f_{\mathrm{ISCO}}} f \, df \, \frac{d^2 \delta\Psi_{e_0,\lambda}(f)}{df^2}. \tag{27}$$

For this, we have considered $f_i = 4$ Hz. The mass of the individual stars is $m_1 = m_2 = 1.4 M_\odot$ with a Λ range of 200 to 1000. From the diagram, we can see that the accumulated dephasing increases with increasing Λ. This is accurate with our previous plots, where the dephasing is larger for $\Lambda = 600$ than for $\Lambda = 400$. In addition, the dephasing also increases for larger e_0, where $e_0 = 0.4$ is

(a) $m_1 = m_2 = 1.4 M_\odot$ and $q = 1$ for $\Lambda = 400$

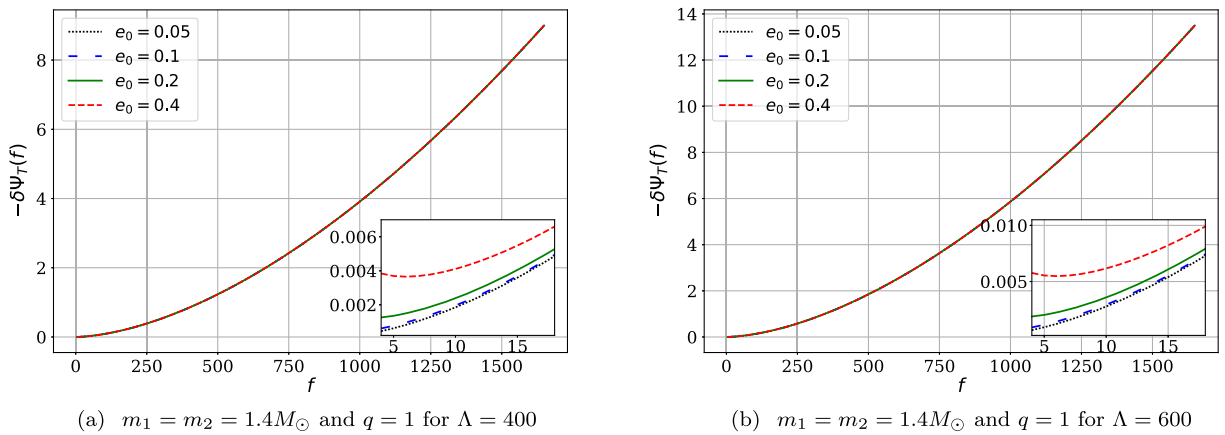(b) $m_1 = m_2 = 1.4 M_\odot$ and $q = 1$ for $\Lambda = 600$

FIG. 2. We show the total tidal phasing $-\delta\Psi_T$ (in radian) for a binary with two $1.4 M_\odot$ neutron stars as a function of gravitational wave frequency f in the range $f_i = 4$ Hz to f_{ISCO}. The initial eccentricities taken for the figure are $e_0 = 0.05, 0.1, 0.2$, and 0.4 with $\Lambda_1 = \Lambda_2 = \Lambda = 400$ and 600 respectively.
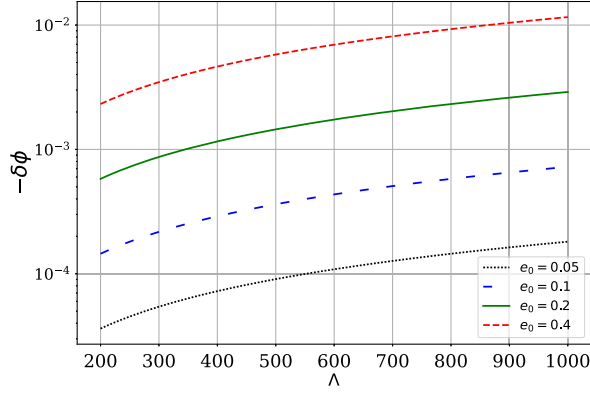
FIG. 3. Shown above is the plot of accumulated dephasing $-\delta\phi$ in radian against dimensionless tidal deformability $\Lambda_1 = \Lambda_2 = \Lambda$ for a binary of identical nonspinning neutron stars of $1.4M_\odot$. The initial eccentricities taken for this system are $e_0 = 0.05, 0.1, 0.2$, and 0.4 with $f_0 = 10$ Hz for the frequency range $f_i = 4$ Hz.

shown to have a larger contribution to the dephasing when compared to other values of e_0. These results precisely reflect the previous results for the dephasing of BNSs. However, the accumulated change is not very high. Dephasing contribution of an effect is indistinguishable from the absence of the effect in the context of scientific measurement if $\delta\phi^2 \leq 1/2\rho^2$, where ρ is the SNR [61,62]. Therefore, dephasing $\delta\phi$ is unobservable if the source does not cross a threshold SNR $\sim (\sqrt{2}\delta\phi)^{-1}$. From Fig. 3, this leads to a required SNR ~ 7000 to observe eccentricity-tide coupling for $e_0 = 0.05$. Therefore, this effect can be observed only with the systems with large eccentricity and very large SNRs in third-generation detectors or beyond.

B. Neutron star–primordial black hole binary

Primordial black holes (PBHs) could have formed in the early phase of the Universe due to the gravitational collapse of large overdensity regions [63–66], e.g., arising from inflation [67–70]. It can possibly explain the fraction of the dark matter (DM). There exist astrophysical and cosmological constraints and clues on their abundance [71–77]. However, these limits and observations are highly model dependent. As a result, the status of PBHs to explain all the DM and GW observations is controversial. Unlike stellar black holes (stellar BHs), there is no physical process preventing the formation of PBHs lighter than the Chandrasekhar mass [78] or in the pair-instability mass gap [79,80]. Therefore, if these objects do exist in nature, it is not unlikely that they can get captured in GW binaries. In this section, we will explore the impact of subsolar mass PBHs in a binary around an NS.

We have demonstrated in the last section that in a BNS, this effect will be hard to measure unless the system has very high eccentricity or/and SNR. However, if the system has a large mass-ratio, the larger body's contribution

dominates, and it is $\propto q$ in the leading order. For this purpose, we explore the impact of this effect on binaries comprising a $1.4M_\odot$ NS and subsolar mass black holes (smBHs).

From Eq. (27), we generate plots for the accumulated dephasing of a nonspinning neutron star-subsolar mass black hole binary with the frequency range $f_i = 4$ Hz to f_{ISCO} [81]. We consider both of the bodies to be nonspinning. The results are shown in Fig. 4. The initial eccentricities taken for these plots are $e_0 = 0.05$ and 0.1, and the Λ range of NS ($\Lambda = \Lambda_1$) is from 100 to 600. Being a BH the companion's Love number vanishes, i.e. $\Lambda_2 = 0$, resulting in a dephasing solely contributed by the NS. From both plots, it can be seen that a larger e_0 corresponds to a larger dephasing effect, which is consistent with the results from other systems. In addition, when comparing both plots, we can see that a larger q also corresponds to a larger dephasing effect, which is expected. We find that even for $e_0 \sim 0.05$ accumulated dephasing can be $\sim \mathcal{O}(0.1)$ radian if $q \sim 10^4$, requiring an SNR $\gtrsim 7$ to be observable.

Therefore, if a high mass-ratio inspiral of this kind is observed then eccentricity-tide coupling will be a measurable effect. However, the capture rates of these systems are likely to be very low [82,83]. During the capture of an smBH, it is likely that the smBH will disrupt the structure of the NS and accrete matter from it. In such a case, observing these binaries may not be possible.

C. Stellar mass exotic compact object–primordial black hole binary

In general relativity (GR), the emergence of new physics is expected to appear in the strong-field regime, when approaching the UV cutoff. Planck-scale modifications of black hole horizons and modification of BH structure have
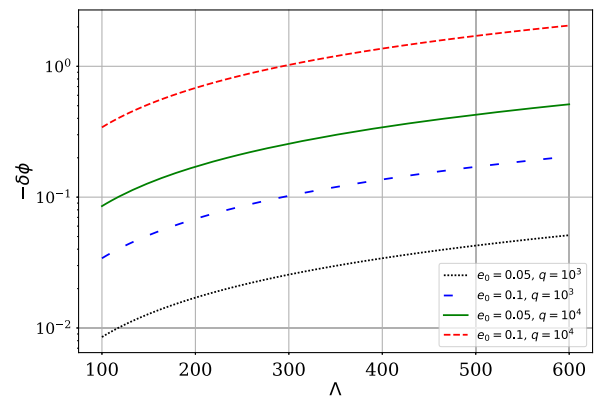

FIG. 4. In the above figure, we show the accumulated dephasing $-\delta\phi$ (in radian) as a function of Λ of a nonspinning NS in a neutron star-subsolar mass black hole binary. NS's mass is $M = 1.4M_\odot$ and the considered mass ratios are $q = 10^3$ and 10^4. The initial eccentricities are $e_0 = 0.05$ and 0.1 with $f_0 = 10$ Hz. We computed the accumulation for the frequency range $f_i = 4$ Hz to f_{ISCO}.

been proposed in several works as resolutions to the information-loss paradox. Among the models of exotic compact objects (ECOs), there are BH polymers, fuzzballs, Firewalls, gravastars, Boson stars etc. to mention a few [84]. BHs in GR have a vanishing Love number [11,85–87]. However, deviation from the classical BH picture in GR introduces nonzero Love numbers. Therefore, the measurement of $\Lambda \neq 0$ will be a smoking gun for deviation from this description.

In the previous sections, we have demonstrated that the eccentricity-tide coupling has a small effect. Since this effect is $\propto \Lambda$, it contributes even lesser for smaller values. However, the effect can become stronger if the systems have a large mass-ratio, as discussed in the previous section. Here, we demonstrate the effect of eccentricity-tide coupling for small values of $\Lambda = \Lambda_1$ of the stellar body when the binary comprises a nonspinning stellar mass and a smBH. Due to the large mass ratio, we ignore the Λ_2 contribution from the smBH.

Figure 5 shows the dephasing for a stellar mass ECO-smBH binary accumulated in the frequency range $f_i = 4$ Hz and f_{ISCO} [81] as a function of Λ in the range 10^{-2} to 1. The total masses for these binaries are (a) $M = 60M_\odot$ and (b) $M = 100M_\odot$ respectively with q value fixed at 10^4. The initial eccentricities taken for this system are $e_0 = 0.05, 0.1, 0.2,$ and 0.4 with an initial frequency $f_0 = 10$ Hz. In these systems the effect can have reasonable dephasing $(\mathcal{O}(0.1))$ radian even for $\Lambda \sim 0.1$ and $e_0 \sim 0.1$. For $e_0 \sim 0.4$ it can even be $\sim \mathcal{O}(10)$ radian. Therefore, if such kind of system is observed with $e_0 \sim 0.05$ then even $\Lambda \sim \mathcal{O}(0.1)$ can lead to the observation of eccentricity-tide coupling if the source has SNR ≥ 7.

D. Extreme mass-ratio inspiral

In this section, we explore the extreme mass-ratio inspiral (EMRIs) comprising spinning supermassive bodies

(SMBs). Extreme mass-ratio inspirals are binaries with very different masses of bodies. We explored this kind of system in the last sections. However, in this section, we focus on EMRIs with SMBs and stellar mass bodies. The frequency of emitted GW by these systems falls in the milliHertz band. These sources will be observed with the future space-based Laser Interferometer Space Antenna (LISA) [88]. Due to the mass-ratio, it will be possible to measure small values of Love numbers $(\Lambda = \Lambda_1)$ of the SMBs [89–91]. It will lead to very accurate and precise testing of the nature of the SMBs. Furthermore, these systems are expected to have large eccentricities. Therefore, if the bodies deviate from the classical BH paradigm, the impact of eccentricity-tide contribution can be significant.

To analyze the contribution of eccentricity to the phase difference of EMRIs, we use Eq. (27) and generate plot for $-\delta\phi$ as a function of Λ accumulated in the frequency range $f_i = 0.4$ mHz to f_{ISCO} [81]. They are demonstrated in Fig. 6. We assumed SMB's spin to be 0.8 which has been used to compute the f_{ISCO}. The initial eccentricities e_0, defined at $f_0 = 1$ mHz, used for these systems are $e_0 = 0.1, 0.2, 0.4,$ and 0.7. The total mass of the extreme mass-ratio inspirals is fixed at $M = 10^6 M_\odot$ with mass-ratio (a) $q = 10^5$ and (b) 5×10^5, representing a $10M_\odot$ BH and a $2M_\odot$ NS, respectively. Due to the mass ratio the impact of the smaller body (Λ_2) is negligible. As expected, the dephasing can be large even for $\Lambda \sim 10^{-3}$. Note, although we assumed e_0^2 to be small to begin with, we have demonstrated the impact of large eccentricity $e_0 = 0.7$. This is just to show the largeness of the eccentricity-tide coupling in these systems. We find that the accumulated dephasing can be $\sim \mathcal{O}(10)$ radian even for $\Lambda \sim 10^{-3}$ and reasonable e_0. In EMRIs of this kind, the orbital eccentricities are expected to have large values. Therefore the values of e_0 considered here are not "unrealistic." However,

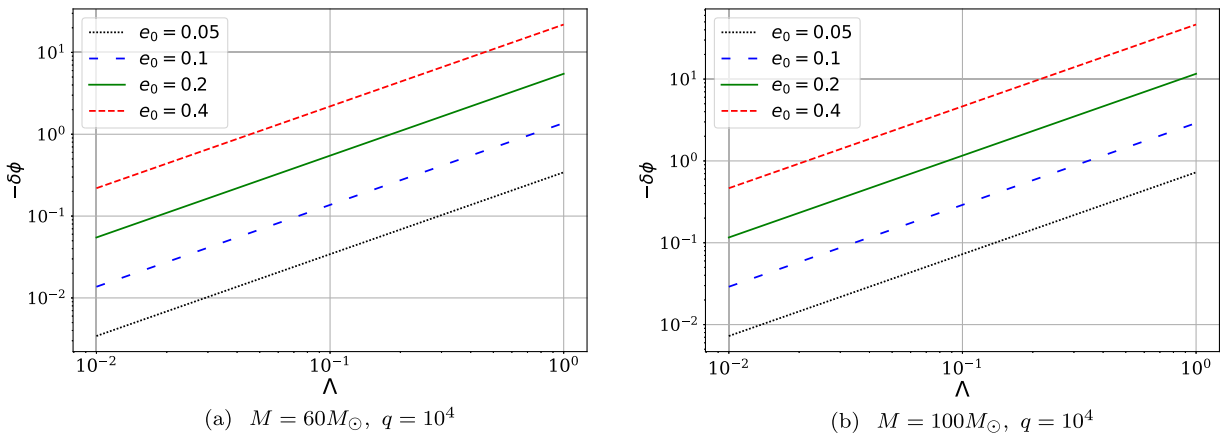(a) $M = 60M_\odot$, $q = 10^4$

(b) $M = 100M_\odot$, $q = 10^4$

FIG. 5. The plots above shows the accumulated dephasing $-\delta\phi$ (in radian) as a function of $\Lambda_1 = \Lambda$ in the range 10^{-2} to 1 for stellar mass ECO-subsolar mass black hole binary. The initial eccentricities taken for these systems are $e_0 = 0.05, 0.1, 0.2,$ and 0.4 with $f_0 = 10$ Hz. The accumulation is computed from $f_i = 4$ Hz to f_{ISCO}.
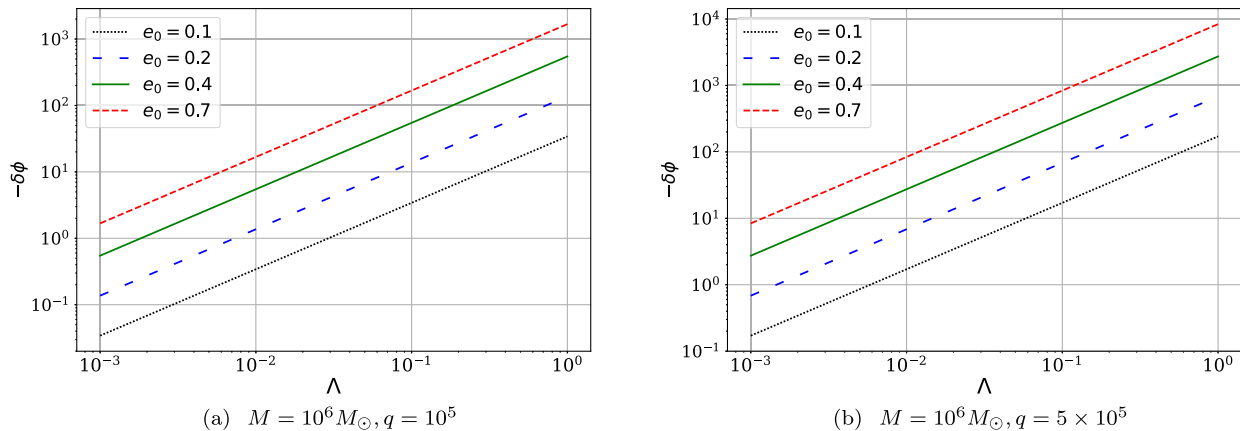
FIG. 6. The figure above shows the accumulated dephasing $-\delta\phi$ (in radian) against $\Lambda_1 = \Lambda$ for extreme mass-ratio inspirals with $M = 10^6 M_\odot$. The initial eccentricities we use are $e_0 = 0.1$, 0.2, 0.4, and 0.7 with $f_0 = 1$ mHz. The SMB has spin $\chi = 0.8$. The accumulation is computed for the frequency range $f_i = 0.4$ mHz to $f_{\rm ISCO}$.

the phase expressions used for the plots are derived assuming a small eccentricity. Therefore, to properly model the effect for high eccentricity systems, much more rigor will be needed in the future.

VI. DISCUSSION AND CONCLUSION

In this paper, we studied the impact of the tidal deformability of a star in an eccentric binary. Assuming a static tide, we found the orbital equations of motion. We assumed the orbits to be eccentric in the absence of the tidal field. Then, we assumed that in the presence of the tide, the orbital motion will change perturbatively. Under such an assumption, we found the solution of the equation of motion in the leading order in eccentricity for the first time. With this newly found result, we computed the total energy of the system and energy flux emitted as GW. Then, we finally calculated the expression of the phase. We found that at the leading order, the phase is proportional to $e_0^2\Lambda$. Due to the nature of the expression, we call it eccentricity-tide coupling. To our knowledge, this is the first time it has been demonstrated that there will be direct coupling between initial eccentricity e_0 and the tidal deformability Λ. In the limit $e_0 = 0$, we recover the result for the tidal contributions in circular binaries, found in [8].

With the result at hand, we plotted the phase for BNSs. We find that the contribution is small for realistic values of eccentricities. We also computed the accumulated dephasing of the system and concluded that it will be measured only for large eccentricities and very large SNRs in third-generation detectors. We also computed the accumulated dephasing in EMRIs. Due to the large mass-ratio, we found that the impact of the effect in the accumulated dephasing becomes larger. We observe that the effect will be measurable if a binary comprising NS and a primordial BH is observed.

Classical BHs in GR have vanishing Love numbers. Measuring a nonzero Love number, therefore, indicates a deviation from the general relativistic BH paradigm. Hence, we computed the impact of eccentricity-tide coupling, assuming small values of tidal deformability for supposed ECOs. EMRIs with stellar mass ECO and smBH have a reasonable contribution to dephasing for realistic eccentricities. Finally, we focus on EMRIs with SMBs at the center. These systems will be observed with the future space-based detector LISA. In these systems, the impact is significant even for very small Λ of SMBs. Since EMRIs are expected to have large eccentricities, large inclinations, and high precession, it will be important to find the contribution of tidal effects in generic orbits targeting these kinds of systems. This, as a result, will provide us a plethora of information regarding the nature of the supermassive compact objects.

While computing the effect of tides in compact stars, the impact on the angular momentum and the consequences thereof has not been explored much. In the current work, we also followed a similar path. This needs more detailed exploration. It remains to see if that can affect the GW emission appreciably. If the angular momentum does affect, then some of the results found in the literature and the current paper may have to be revisited. We will look into it in detail in the future.

Since we have considered the static tide, we ignored the impact of the mode excitations explored in Refs. [41,43,44]. It will be interesting to model such effects analytically so that it becomes useful in the observational context. We leave such an endeavor for the future.

[1] J. Aasi *et al.* (LIGO Scientific Collaboration), Advanced LIGO, Classical Quantum Gravity **32**, 074001 (2015).

[2] F. Acernese *et al.* (Virgo Collaboration), Advanced Virgo: A second-generation interferometric gravitational wave detector, Classical Quantum Gravity **32**, 024001 (2015).

[3] B. P. Abbott *et al.* (LIGO Scientific and Virgo Collaborations), GW170817: Observation of gravitational waves from a binary neutron star inspiral, Phys. Rev. Lett. **119**, 161101 (2017).

[4] B. P. Abbott *et al.* (LIGO Scientific and Virgo Collaborations), GW170817: Measurements of neutron star radii and equation of state, Phys. Rev. Lett. **121**, 161101 (2018).

[5] B. P. Abbott *et al.* (LIGO Scientific and Virgo Collaborations), GW190425: Observation of a compact binary coalescence with total mass $\sim 3.4 M_\odot$, Astrophys. J. Lett. **892**, L3 (2020).

[6] B. P. Abbott *et al.* (LIGO Scientific and Virgo Collaborations), Properties of the binary neutron star merger GW170817, Phys. Rev. X **9**, 011001 (2019).

[7] B. P. Abbott *et al.* (LIGO Scientific, Virgo, Fermi-GBM, and INTEGRAL Collaborations), Gravitational waves and gamma-rays from a binary neutron star merger: GW170817 and GRB 170817A, Astrophys. J. Lett. **848**, L13 (2017).

[8] E. E. Flanagan and T. Hinderer, Constraining neutron star tidal Love numbers with gravitational wave detectors, Phys. Rev. D **77**, 021502 (2008).

[9] T. Hinderer, Tidal Love numbers of neutron stars, Astrophys. J. **677**, 1216 (2008).

[10] T. Damour and A. Nagar, Relativistic tidal properties of neutron stars, Phys. Rev. D **80**, 084035 (2009).

[11] T. Binnington and E. Poisson, Relativistic theory of tidal Love numbers, Phys. Rev. D **80**, 084018 (2009).

[12] P. Char and S. Datta, Relativistic tidal properties of superfluid neutron stars, Phys. Rev. D **98**, 084010 (2018).

[13] S. Datta and P. Char, Effect of superfluid matter of neutron star on the tidal deformability, Phys. Rev. D **101**, 064016 (2020).

[14] B. Biswas and S. Bose, Tidal deformability of an anisotropic compact star: Implications of GW170817, Phys. Rev. D **99**, 104002 (2019).

[15] B. Biswas, R. Nandi, P. Char, and S. Bose, Role of crustal physics in the tidal deformation of a neutron star, Phys. Rev. D **100**, 044056 (2019).

[16] F. Gittins, N. Andersson, and J. P. Pereira, Tidal deformations of neutron stars with elastic crusts, Phys. Rev. D **101**, 103025 (2020).

[17] M. C. Miller *et al.*, PSR J0030 + 0451 mass and radius from NICER data and implications for the properties of neutron star matter, Astrophys. J. Lett. **887**, L24 (2019).

[18] T. E. Riley *et al.*, A NICER view of PSR J0030 + 0451: Millisecond pulsar parameter estimation, Astrophys. J. Lett. **887**, L21 (2019).

[19] M. C. Miller *et al.*, The radius of PSR J0740 + 6620 from NICER and XMM-Newton data, Astrophys. J. Lett. **918**, L28 (2021).

[20] T. E. Riley *et al.*, A NICER view of the massive pulsar PSR J0740 + 6620 informed by radio timing and XMM-Newton spectroscopy, Astrophys. J. Lett. **918**, L27 (2021).

[21] J. Antoniadis *et al.*, A massive pulsar in a compact relativistic binary, Science **340**, 6131 (2013).

[22] H. T. Cromartie *et al.*, Relativistic Shapiro delay measurements of an extremely massive millisecond pulsar, Nat. Astron. **4**, 72 (2019).

[23] E. Fonseca *et al.*, Refined mass and geometric measurements of the high-mass PSR J0740 + 6620, Astrophys. J. Lett. **915**, L12 (2021).

[24] I. M. Romero-Shaw, N. Farrow, S. Stevenson, E. Thrane, and X.-J. Zhu, On the origin of GW190425, Mon. Not. R. Astron. Soc. **496**, L64 (2020).

[25] A. K. Lenon, A. H. Nitz, and D. A. Brown, Measuring the eccentricity of GW170817 and GW190425, Mon. Not. R. Astron. Soc. **497**, 1966 (2020).

[26] D. Bini, T. Damour, and G. Faye, Effective action approach to higher-order relativistic tidal interactions in binary systems and their effective one body description, Phys. Rev. D **85**, 124034 (2012).

[27] T. Damour, A. Nagar, and L. Villain, Measurability of the tidal polarizability of neutron stars in late-inspiral gravitational-wave signals, Phys. Rev. D **85**, 123007 (2012).

[28] A. Maselli, L. Gualtieri, F. Pannarale, and V. Ferrari, On the validity of the adiabatic approximation in compact binary inspirals, Phys. Rev. D **86**, 044032 (2012).

[29] J. Vines, E. E. Flanagan, and T. Hinderer, Post-1-Newtonian tidal effects in the gravitational waveform from binary inspirals, Phys. Rev. D **83**, 084051 (2011).

[30] J. E. Vines and E. E. Flanagan, Post-1-Newtonian quadrupole tidal interactions in binary systems, Phys. Rev. D **88**, 024046 (2013).

[31] J. Steinhoff, T. Hinderer, A. Buonanno, and A. Taracchini, Dynamical tides in general relativity: Effective action and effective-one-body Hamiltonian, Phys. Rev. D **94**, 104028 (2016).

[32] J. Steinhoff, T. Hinderer, T. Dietrich, and F. Foucart, Spin effects on neutron star fundamental-mode dynamical tides: Phenomenology and comparison to numerical simulations, Phys. Rev. Res. **3**, 033129 (2021).

[33] P. Schmidt and T. Hinderer, Frequency domain model of f-mode dynamic tides in gravitational waveforms from compact binary inspirals, Phys. Rev. D **100**, 021501 (2019).

[34] G. Pratten, P. Schmidt, and T. Hinderer, Gravitational-wave asteroseismology with fundamental modes from compact binary inspirals, Nat. Commun. **11**, 2553 (2020).

[35] P. Pani, L. Gualtieri, and V. Ferrari, Tidal Love numbers of a slowly spinning neutron star, Phys. Rev. D **92**, 124003 (2015).

[36] P. Landry, Tidal deformation of a slowly rotating material body: Interior metric and Love numbers, Phys. Rev. D **95**, 124058 (2017).

[37] T. Abdelsalhin, L. Gualtieri, and P. Pani, Post-Newtonian spin-tidal couplings for compact binaries, Phys. Rev. D **98**, 104046 (2018).

[38] G. Castro, L. Gualtieri, A. Maselli, and P. Pani, Impact and detectability of spin-tidal couplings in neutron star inspirals, Phys. Rev. D **106**, 024011 (2022).

[39] D. Reitze *et al.*, Cosmic Explorer: The U.S. contribution to gravitational-wave astronomy beyond LIGO, Bull. Am. Astron. Soc. **51**, 035 (2019).

[40] M. Maggiore, C. Van Den Broeck, N. Bartolo, E. Belgacem, D. Bertacca, M. A. Bizouard, M. Branchesi, S. Clesse,

S. Foffa, J. García-Bellido *et al.*, Science case for the Einstein Telescope, J. Cosmol. Astropart. Phys. 03 (2020) 050.

[41] W. Xu and D. Lai, Resonant tidal excitation of oscillation modes in merging binary neutron stars: Inertial-gravity modes, Phys. Rev. D **96**, 083005 (2017).

[42] H. Yang, W. E. East, V. Paschalidis, F. Pretorius, and R. F. P. Mendes, Evolution of highly eccentric binary neutron stars including tidal effects, Phys. Rev. D **98**, 044007 (2018).

[43] H. Yang, Inspiralling eccentric binary neutron stars: Orbital motion and tidal resonance, Phys. Rev. D **100**, 064023 (2019).

[44] J.-S. Wang and D. Lai, Evolution of inspiralling neutron star binaries: Effects of tidal interactions and orbital eccentricities, Phys. Rev. D **102**, 083005 (2020).

[45] P. C. Peters and J. Mathews, Gravitational radiation from point masses in a Keplerian orbit, Phys. Rev. **131**, 435 (1963).

[46] B. Moore, M. Favata, K. G. Arun, and C. K. Mishra, Gravitational-wave phasing for low-eccentricity inspiralling compact binaries to 3PN order, Phys. Rev. D **93**, 124061 (2016).

[47] K. G. Arun, L. Blanchet, B. R. Iyer, and S. Sinha, Third post-Newtonian angular momentum flux and the secular evolution of orbital elements for inspiralling compact binaries in quasi-elliptical orbits, Phys. Rev. D **80**, 124018 (2009).

[48] B. P. Abbott *et al.* (LIGO Scientific and Virgo Collaborations), GW170817: Measurements of neutron star radii and equation of state, Phys. Rev. Lett. **121**, 161101 (2018).

[49] B. Biswas and S. Datta, Constraining neutron star properties with a new equation of state insensitive approach, Phys. Rev. D **106**, 043012 (2022).

[50] L. Wen, On the eccentricity distribution of coalescing black hole binaries driven by the Kozai mechanism in globular clusters, Astrophys. J. **598**, 419 (2003).

[51] N. Seto, Highly eccentric Kozai mechanism and gravitational-wave observation for neutron star binaries, Phys. Rev. Lett. **111**, 061106 (2013).

[52] F. Antonini, S. Toonen, and A. S. Hamers, Binary black hole mergers from field triples: Properties, rates and the impact of stellar evolution, Astrophys. J. **841**, 77 (2017).

[53] C. L. Rodriguez and F. Antonini, A triple origin for the heavy and low-spin binary black holes detected by LIGO/ Virgo, Astrophys. J. **863**, 7 (2018).

[54] J. Samsing and E. Ramirez-Ruiz, On the assembly rate of highly eccentric binary black hole mergers, Astrophys. J. Lett. **840**, L14 (2017).

[55] J. Samsing, Eccentric black hole mergers forming in globular clusters, Phys. Rev. D **97**, 103014 (2018).

[56] B. Liu and D. Lai, Enhanced black hole mergers in binary–binary interactions, Mon. Not. R. Astron. Soc. **483**, 4060 (2019).

[57] B.-M. Hoang, S. Naoz, B. Kocsis, F. A. Rasio, and F. Dosopoulou, Black hole mergers in galactic nuclei induced by the eccentric Kozai–Lidov effect, Astrophys. J. **856**, 140 (2018).

[58] W. E. East, S. T. McWilliams, J. Levin, and F. Pretorius, Observing complete gravitational wave signals from dynamical capture binaries, Phys. Rev. D **87**, 043004 (2013).

[59] M. Favata, C. Kim, K. G. Arun, J. Kim, and H. W. Lee, Constraining the orbital eccentricity of inspiralling compact binary systems with Advanced LIGO, Phys. Rev. D **105**, 023003 (2022).

[60] E. E. Flanagan and T. Hinderer, Constraining neutron-star tidal love numbers with gravitational-wave detectors, Phys. Rev. D **77**, 021502 (2008).

[61] E. E. Flanagan and S. A. Hughes, Measuring gravitational waves from binary black hole coalescences: 2. The waves' information and its extraction, with and without templates, Phys. Rev. D **57**, 4566 (1998).

[62] L. Lindblom, B. J. Owen, and D. A. Brown, Model waveform accuracy standards for gravitational wave data analysis, Phys. Rev. D **78**, 124020 (2008).

[63] Ya. B. Zel'dovich and I. D. Novikov, The hypothesis of cores retarded during expansion and the hot cosmological model, Sov. Astron. **10**, 602 (1967), https://ui.adsabs .harvard.edu/abs/1967SvA....10..602Z/abstract.

[64] S. Hawking, Gravitationally collapsed objects of very low mass, Mon. Not. R. Astron. Soc. **152**, 75 (1971).

[65] B. J. Carr and S. W. Hawking, Black holes in the early Universe, Mon. Not. R. Astron. Soc. **168**, 399 (1974).

[66] G. F. Chapline, Cosmological effects of primordial black holes, Nature (London) **253**, 251 (1975).

[67] B. J. Carr and J. E. Lidsey, Primordial black holes and generalized constraints on chaotic inflation, Phys. Rev. D **48**, 543 (1993).

[68] P. Ivanov, P. Naselsky, and I. Novikov, Inflation and primordial black holes as dark matter, Phys. Rev. D **50**, 7173 (1994).

[69] J. Garcia-Bellido, A. D. Linde, and D. Wands, Density perturbations and black hole formation in hybrid inflation, Phys. Rev. D **54**, 6040 (1996).

[70] H. I. Kim and C. H. Lee, Constraints on the spectral index from primordial black holes, Phys. Rev. D **54**, 6001 (1996).

[71] B. Carr, F. Kuhnel, and M. Sandstad, Primordial black holes as dark matter, Phys. Rev. D **94**, 083504 (2016).

[72] B. J. Carr, K. Kohri, Y. Sendouda, and J. Yokoyama, New cosmological constraints on primordial black holes, Phys. Rev. D **81**, 104019 (2010).

[73] B. Carr, K. Kohri, Y. Sendouda, and J. Yokoyama, Constraints on primordial black holes, Rep. Prog. Phys. **84**, 116902 (2021).

[74] B. Carr and F. Kuhnel, Primordial black holes as dark matter: Recent developments, Annu. Rev. Nucl. Part. Sci. **70**, 355 (2020).

[75] A. M. Green and B. J. Kavanagh, Primordial black holes as a dark matter candidate, J. Phys. G **48**, 043001 (2021).

[76] A. Escrivà, F. Kuhnel, and Y. Tada, Primordial black holes, arXiv:2211.05767.

[77] B. Carr, S. Clesse, J. García-Bellido, and F. Kühnel, Cosmic conundra explained by thermal history and primordial black holes, Phys. Dark Universe **31**, 100755 (2021).

[78] S. Chandrasekhar, The maximum mass of ideal white dwarfs, Astrophys. J. **74**, 81 (1931).

[79] G. Rakavy and G. Shaviv, Instabilities in highly evolved stellar models, Astrophys. J. **148**, 803 (1967).

[80] G. S. Farley, Supernovae explosions induced by pair-production instability, Astrophys. Space Sci. **2**, 96 (1968).

[81] A. Taracchini, A. Buonanno, S. A. Hughes, and G. Khanna, Modeling the horizon-absorbed gravitational flux for equatorial-circular orbits in Kerr spacetime, Phys. Rev. D **88,** 044001 (2013); **88,** 109903(E) (2013).

[82] F. Capela, M. Pshirkov, and P. Tinyakov, Constraints on primordial black holes as dark matter candidates from capture by neutron stars, Phys. Rev. D **87,** 123524 (2013).

[83] Y. Génolini, P. Serpico, and P. Tinyakov, Revisiting primordial black hole capture into neutron stars, Phys. Rev. D **102,** 083004 (2020).

[84] V. Cardoso, E. Franzin, and P. Pani, Is the gravitational-wave ringdown a probe of the event horizon?, Phys. Rev. Lett. **116,** 171101 (2016); **117,** 089902(E) (2016).

[85] P. Landry and E. Poisson, Relativistic theory of surficial Love numbers, Phys. Rev. D **89,** 124011 (2014).

[86] A. Le Tiec, M. Casals, and E. Franzin, Tidal Love numbers of Kerr black holes, Phys. Rev. D **103,** 084021 (2021).

[87] H. S. Chia, Tidal deformation and dissipation of rotating black holes, Phys. Rev. D **104,** 024013 (2021).

[88] P. Amaro-Seoane *et al.* (LISA Collaboration), Laser interferometer space antenna, arXiv:1702.00786.

[89] P. Pani and A. Maselli, Love in extrema ratio, Int. J. Mod. Phys. D **28,** 1944001 (2019).

[90] S. Datta, Probing horizon scale quantum effects with Love, Classical Quantum Gravity **39,** 225016 (2022).

[91] G. A. Piovano, A. Maselli, and P. Pani, Constraining the tidal deformability of supermassive objects with extreme mass ratio inspirals and semianalytical frequency-domain waveforms, Phys. Rev. D **107,** 024021 (2023).